COMMUNICATION

Check for updates

A hollow Ag/AgCl nanoelectrode for single-cell chloride detection†

Tian-Yang Zhang, Fang-Qing Liu, Zheng Li, Yi-Tong Xu, [ID] Wei-Wei Zhao, [ID] * Hong-Yuan Chen and Jing-Juan Xu [ID] *

This work reports the construction of a miniaturized Ag/AgCl nanoelectrode on a nanopipette, which is capable of dual-functions of single-cell drug infusion and chloride detection and is envisioned to promote the study of chloride-correlated therapeutic effects.

The homeostatic regulation of inorganic cations and anions is a characteristic of healthy cells. Steady-state maintenance of this ionic homeostasis across the entire intracellular fluid is critical for normal cellular functions and life processes.[1] Among various physiological ions, chloride is the predominant and one of the most important anions in our body. Regulated by the transmembrane ion channel and cotransporters, the normal cytosolic chloride concentration is approximately 5–40 mM *versus* the high extracellular value of *ca.* 120 mM.[2–4] Increasing evidence demonstrates that chloride serves many fundamental biological roles in *e.g.* cell cycle progression and proliferation, regulation of gene expression, water secretion, *etc.*[5–7] In particular, the disturbances of cytosolic chloride have been correlated closely with cellular apoptosis and many pathological alterations.[6]

Small molecular drugs capable of regulating cytosolic chloride concentrations have attracted substantial efforts.[4,8] However, in traditional studies, only results with population averaging were obtained. To elucidate the accurate therapeutic-action and decipher the associated fundamental cellular physiology,[9] the precise knowledge of how a specific therapeutic reagent and its dosage affect the cytosolic chloride within single cells is highly demanded. This highlights the significance of single-cell techniques capable of sensitive cytosolic modulation and chloride detection. So far, researchers still lack such a bifunctional nanotool that is highly accessible, stable and durable.

To this end, solid nanoprobes that are able to intrude single live cells and perform electrochemical detection in a

Key Laboratory of Analytical Chemistry for Life Science, School of Chemistry and Chemical Engineering, Nanjing University, Nanjing 210023, China.
E-mail: zww@nju.edu.cn, xujj@nju.edu.cn

† Electronic supplementary information (ESI) available. See DOI: https://doi.org/10.1039/d3cc06078k

biocompatible and biorthogonal manner is of particular interest.[10–12] Although many endogenous species have been addressed using carbonic or metallic nanoelectrodes,[13,14] potential-resolved electrochemistry towards chloride remains a major challenge. Extra major challenges are their impotence for simultaneous drug delivery and chloride detection in an *in situ* manner.

Remarkably, nanopipettes have been increasingly explored for single-cell electroanalysis (Table S1, ESI†).[15–18] Various "metallic redox indicators" were initially derived for faradaic detection of redox-active species,[5–7,19–21] while the lumens of the nanopipettes were utilized for custom functionalization and accommodation[22,23] and on-demand collection and injection.[20,24–26] Also based on faradaic reactions, photoelectrochemistry and electrochemiluminescence[27] techniques were grafted to nanopipettes for single-cell analysis.[28,29] Meanwhile, iontronic single-cell nanotools have also been developed for addressing non-electrogenic species.[30–32] Considering the importance of physiological chloride, we reason that properly engineered nanopipette "electrodes of the second kind", *e.g.* silver/silver-chloride (Ag/AgCl) nanopipettes, might open the possibility for single-cell chloride detection.

Herein, a hollow Ag/AgCl nanopipette capable of cytosolic chloride detection and drug injection was devised (see ESI† for experimental details). Specifically, as illustrated in Fig. 1a, sequential Ti and Ag deposition *via* magnetron sputtering and chemical oxidation were conducted to *in situ* form a AgCl/Ag film as the chloride-sensitive and metal contact layers. The as-formed nanotool was subsequently protected by a selected polymeric anti-interference layer of polyacrylonitrile (PAN), succeeded by wax sealing to fix a specific exposure. In such a nanoarchitecture, the innermost glass lumen could be used for drug delivery, the underlying metal contact layer for wiring to the external circuit and the nanoscale Ag/AgCl with excellent electrochemical stability for single-cell chloride detection; while the outermost PAN was selected as the protecting layer due to its good capability against various biological interferents while retaining good ion permeability. Upon exposure to
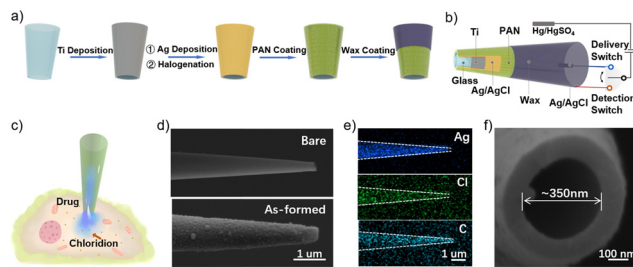
Fig. 1 (a) Preparation of the hollow Ag/AgCl nanoelectrode. (b) The detailed perspective of the nanotool with cytosolic injection and detection circuits. (c) Scheme of cytomembrane penetration and injection of specific therapeutic agents and chloride detection within a single cell. (d) The side-view SEM images of the as-pulled (upper) and as-devised (bottom) nanotool. Scale bar = 1 μm. (e) The corresponding elemental mapping images. Scale bar = 1 μm. (f) The top-view SEM images of the as-devised nanotool. Scale bar = 100 nm.
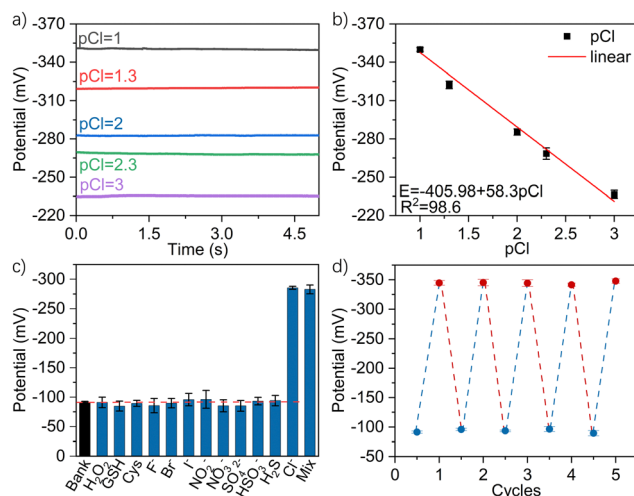

Fig. 2 (a) Potential responses in HEPES milieus with different chloride concentrations within the range from 1–100 mV. (b) The corresponding derived linearity of log pCl vs. potential (vs. Hg/Hg$_2$SO$_4$) (mV). (c) Selectivity tests towards various interfering species and the mixed sample. (d) Recycling potential responses of the nanotool measured in the HEPES milieu without and with 100 mM chloridion. Error bars represent standard deviations from 3 independent detections.

chloride, the altered chloride concentrations will result in different electrode potentials based on the Nernst equation.[33]

For cellular application, as depicted in Fig. 1b and c, by the alternate connection of the delivery and detection switch, this nanotool could perform chloride-oriented drug administration and precise study of the corresponding therapeutic-action. Note that a Hg/Hg$_2$SO$_4$ electrode was used as the reference electrode because it is not sensitive to the ambient chloride. Besides, as the intracellular drug delivery was enabled by electroosmosis and chloride detection followed the principle of the Nernst equation, there were no faradaic currents throughout the experiments, ensuring the minimized perturbation to the target cells. Fig. 1d shows the scanning electron microscope (SEM) images of the pristine as-pulled nanopipette (upper) and the as-fabricated Ag/AgCl nanoelectrode (bottom), respectively. As shown, the pristine nanopipette possessed a near-cylindrical shape with a rather smooth surface, whereas the Ag/AgCl nanoelectrode exhibited a rough surface consisting of numerous AgCl nanoparticles. Incidentally, upon identical preparation upon a plane surface, the nanoscale AgCl was also characterized by an atomic force microscope (Fig. S1, ESI†). Note that the coverage of PAN film could not be recorded by SEM due to the strong contrast, which was then confirmed by elemental mapping showing the stepwise appearance of Ag, Cl, and C elements, as recorded in Fig. 1e. For better clarity, it was further verified by electrochemical impedance spectroscopy (EIS), as discussed with Fig. S2 (ESI†). Fig. 1f shows the quasi-circular aperture of ca. 350 nm for following cytosolic delivery.

The feasibility of this nanotool for practical usage was then *in vitro* investigated. According to its basic working principle, the potential of the Ag/AgCl nanoelectrode is controlled by the chloridion concentration in the electrolyte. The responses of the nanotool were initially recorded within the HEPES milieu of variable chloride concentrations. As shown in Fig. 2a, distinct and stable open-circuit-potential curves were obtained, with the respective values of ca. −350 mV, −320 mV, −285 mV, −267 mV and −235 mV corresponding to chloridion concentrations of 100 mM (pCl = 1), 50.11 mM (pCl = 1.3), 10 mM (pCl = 2), 5.01 mM (pCl = 2.3) and 1 mM (pCl = 3), respectively. Fig. 2b

shows the derived linear relationship between the potentials and the corresponding chloridion concentration, with the regression equation of $E = -405.98 + 58.3$ pCl ($R^2 = 98.6$). Significantly, the range of linearity would be ideal for cellular applications given the cytosolic chloridion of ca. 5–40 mM.[3] Considering the interference, halide ions are generally less than 10^{-8} M[34,35] in normal cytosols, and the anti-interference capability of the nanotool was then studied by detecting 10 mM chloridion against the interferents of halide ions, some common anions[36–39] and intracellular species,[20,40] including 10^{-8} M F$^-$, 10^{-8} M Br$^-$, 10^{-8} M I$^-$, 100 mM NO$_2^-$, 100 mM NO$_3^-$, 100 mM SO$_4^{2-}$, 10^{-6} M H$_2$S, 1 mM H$_2$O$_2$, 1 mM GSH and 1 mM cysteine as well as their mixture. As shown in Fig. 2c, only chloridions and the mixture could induce obvious and similar potential changes of ca. −283 mV, indicating its good selectivity for potential cytosolic probing. Next, recycling potential measurements of the nanotool were performed in the HEPES milieu in the absence and presence of 100 mM chloridion. As shown in Fig. 2d, the highly recyclable potential responses validated the good operational stability and precision for repeated usage. Incidentally, as shown in Fig. S3 (ESI†), the long-term durability of this nanotool was also demonstrated by 1000s detection within the HEPES milieu with 100 mM chloridion. Besides, the effect of possible pH fluctuation was studied using HEPES milieu containing 10 mM chloridion with pH of 6.4, 7.4, and 8.0. Fig. S4 (ESI†) indicates the negligible pH effect on the nanotool. In addition, the possible adsorption effect was further studied by dipping the nanotool into cell lysate for 15 min before testing. As shown in Fig. S5 (ESI†), the quite stable signals disclosed the minimal adsorption effect of the nanotool.

The nanotool was then implemented for *in situ* intracellular drug delivery and chloridion detection within a single MCF-7 cell.
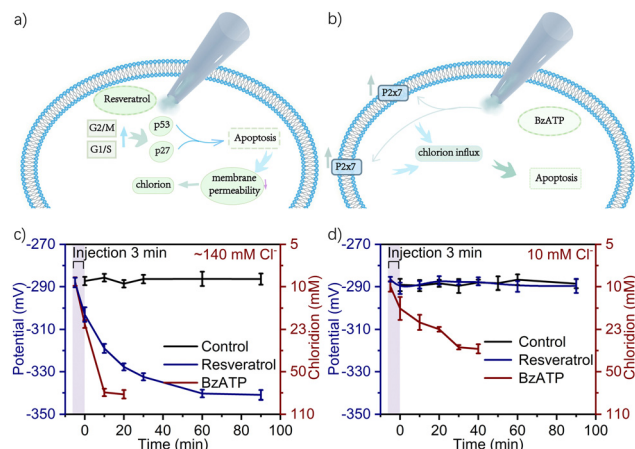
Fig. 3 Signalling routes of (a) resveratrol and (b) BzATP-induced apoptosis. The evolution of recorded potential and corresponding intracellular chloride level MCF-7 cells treated by electroosmotic delivery of 100 μM resveratrol and BzATP under +1 V for 3 min, with extracellular chloridion set as (c) ~140 mM and (d) 10 mM. Error bars represent standard deviations from 10 independent detections.

Resveratrol and 2′-3′-O-(4-benzoylbenzoyl)-ATP (BzATP) were selected as a representative apoptosis drug and chloride influx drug, respectively. As illustrated in Fig. 3a, resveratrol could upgrade the expression and kinase activities of positive G1/S and G2/M regulators, which in the presence of high levels of p27 and p53 could lead to cell cycle blockade at the S-phase and induction of early stage apoptosis with a corresponding change of membrane permeability for chloridion influx.[41] By contrast, as shown in Fig. 3b, BzATP as a P2X7 receptor agonist could lead to activation of P2X7, inducing depolarization of the membrane potential and direct chloridion influx towards apoptosis.[42] The biocompatible electroosmotic intracellular delivery had previously been verified by the delivery of fluorescein isothiocyanate (FITC),[16,20] and the same function of the present nanodevice was also validated as shown in Figure S6–S9 (ESI†).

Within the normal 1× PBS containing ca. 140 mM chloridion as the extracellular environment[3,7] and upon electroosmotic delivery of 100 μM resveratrol and BzATP for 1 min under +1 V, the evolution of intracellular chloridion levels was recorded based on 10 MCF-7 cells per group. As shown in Fig. S10 (ESI†) for the case of resveratrol, the potential gradually declined from ca. −285 mV to −340 mV over a duration of 90 min and then tended to an equilibrium, corresponding to chloridion levels from ca. 8 mM to 74 mM. However, for the case of BzATP, the potential declined from ca. −287 mV to −341 mV within 30 min, corresponding to the chloridion levels from ca. 9 mM to 77 mM. Such results indicated that BzATP enabled a more rapid onset of action in chloridion influx. To further reveal its potential in yielding precise knowledge of how does a specific drug with specific therapeutic dosages affect the cytosolic chloride, electroosmotic infusion of 100 μM resveratrol and BzATP under +1 V was then respectively conducted for 2 min and 3 min. As shown in Fig. S10 (ESI†) and Fig. 3c, with the increase of the delivery time, the rate of potential decline increased and the potential

approached its equilibrium faster. As shown, upon 3 min infusion of resveratrol, the potential declined from ca. −285 mV to −340 mV rapidly within ca. 60 min. For the case of BzATP, the potential declined from ca. −285 mV to −341 mV and even reduced to ca. 10 min.

Subsequently, the extracellular chloridion was set as 10 mM[10] and the electroosmotic delivery was conducted for 3 min with other conditions unchanged, the evolution of intracellular chloridion levels was then recorded. As shown in Fig. 3d, resveratrol could hardly induce alternation of the intracellular chloridion level, whereas BzATP could still cause obvious chloridion influx, indicating the different roles of the two drugs in the signal transduction pathways of the treated cells. These results demonstrated the feasibility of this nanodevice for bifunctional chloride-oriented therapeutics at a single-cell level, i.e. not only direct intracellular drug administration with high precision but also in situ evaluation of the therapeutic-action with high sensitivity. Incidentally, the corresponding cellular status of the above experiments was simultaneously monitored using the fluorescent dye of Hoechest 33342, as discussed in Fig. S11–S20 (ESI†).

In summary, a nanopipette-derived hollow Ag/AgCl nanoelectrode was devised. The as-fabricated nanodevice was validated to be dual-functional, capable of cytosolic drug infusion and chloride detection within a single cell. We also show that this nanodevice possesses proper sensitivity, selectivity, and stability for probing cytosolic chloride in a time-resolved manner. It was further used to evaluate the therapeutic-action of a specific chloride-targeted drug and its dosage down to the single-cell level, which differed from the methodologies normally performed at a population level (Tables S2 and S3, ESI†). This work is envisaged to deepen our understanding of how the chloride fluxes are physiologically regulated by different cells upon the application of external chemotherapies.

Conflicts of interest

The authors declare no conflict of interest.

Notes and references

1 D. Aksentijević, A. Karlstaedt, M. V. Basalay, B. A. O'Brien, D. Sanchez-Tatay, S. Eminaga, A. Thakker, D. A. Tennant, W. Fuller, T. R. Eykyn, H. Taegtmeyer and M. J. Shattock, Nat. Commun., 2020, 11, 4337.
2 T. Stauber and T. J. Jentsch, Annu. Rev. Physiol., 2013, 75, 453–477.
3 N. Busschaert, S. H. Park, K. H. Baek, Y. P. Choi, J. Park, E. N. W. Howe, J. R. Hiscock, L. E. Karagiannidis, I. Marques, V. Félix, W. Namkung, J. L. Sessler, P. A. Gale and I. Shin, Nat. Chem., 2017, 9, 667–675.
4 S. K. Ko, S. K. Kim, A. Share, V. M. Lynch, J. Park, W. Namkung, W. Van Rossom, N. Busschaert, P. A. Gale, J. L. Sessler and I. Shin, Nat. Chem., 2014, 6, 885–892.
5 T. J. Jentsch, K. Steinmeyer and G. Schwarz, Nature, 1990, 348, 510–514.
6 S. Hosogi, K. Kusuzaki, T. Inui, X. Wang and Y. Marunaka, J. Cell. Mol. Med., 2014, 18, 1124–1133.

7 T. J. Jentsch and M. Pusch, *Physiol. Rev.*, 2018, **98**, 1493–1590.

8 H. L. Chen, Y. J. Liu, X. B. Cheng, S. Fang, Y. Sun, Z. Yang, W. Zheng, X. Ji and Z. Wu, *Angew. Chem., Int. Ed.*, 2021, **60**, 10833–10841.

9 S. O. Kelley, C. A. Mirkin, D. R. Walt, R. F. Ismagilov, M. Toner and E. H. Sargent, *Nat. Nanotechnol.*, 2014, **9**, 969–980.

10 N. T. N. Phan, X. Li and A. G. Ewing, *Nat. Rev. Chem.*, 2017, **1**, 0048.

11 Y. L. Ying, Y. X. Hu, R. Gao, R. J. Yu, Z. Gu, L. P. Lee and Y. T. Long, *J. Am. Chem. Soc.*, 2018, **140**, 5385–5392.

12 Y. L. Zhao, S. S. You, A. Q. Zhang, J. H. Lee, J. L. Huang and C. M. Lieber, *Nat. Nanotechnol.*, 2019, **14**, 783–790.

13 X. W. Zhang, Q. F. Qiu, H. Jiang, F. L. Zhang, Y. L. Liu, C. Amatore and W. H. Huang, *Angew. Chem., Int. Ed.*, 2017, **56**, 12997–13000.

14 K. K. Hu, Y. Li, S. A. Rotenberg, C. Amatore and M. V. Mirkin, *J. Am. Chem. Soc.*, 2019, **141**, 4564–4568.

15 W. Zhu, C. Gu, J. Dunevall, L. Ren, X. Zhou and A. G. Ewing, *Angew. Chem., Int. Ed.*, 2019, **58**, 4238–4242.

16 R. J. Yu, Y. L. Ying, R. Gao and Y. T. Long, *Angew. Chem., Int. Ed.*, 2019, **58**, 3706–3714.

17 B. P. Nadappuram, P. Cadinu, A. Barik, A. J. Ainscough, M. J. Devine, M. Kang, J. Gonzalez-Garcia, J. T. Kittler, K. R. Willison, R. Vilar, P. Actis, B. Wojciak-Stothard, S.-H. Oh, A. P. Ivanov and J. B. Edel, *Nat. Nanotechnol.*, 2019, **14**, 80–88.

18 Q. W. Yue, X. C. Li, F. Wu, W. Ji, Y. Zhang, P. Yu, M. Zhang, W. Ma, M. Wang and L. Mao, *Angew. Chem., Int. Ed.*, 2020, **59**, 11061–11065.

19 X. Li, Y. Jin, F. H. Zhu, R. Liu, Y. Jiang, Y. Jiang and L. Mao, *Angew. Chem., Int. Ed.*, 2022, **61**, e202208121.

20 Y. F. Ruan, F. Z. Chen, Y. T. Xu, T. Y. Zhang, S. Y. Yu, W. W. Zhao, D. Jiang, H.-Y. Chen and J.-J. Xu, *Angew. Chem., Int. Ed.*, 2021, **60**, 25762–25765.

21 A. Picollo and M. Pusch, *Nature*, 2005, **436**, 420–423.

22 R. R. Pan, K. K. Hu, D. C. Jiang, U. Samuni and M. V. Mirkin, *J. Am. Chem. Soc.*, 2019, **141**, 19555–19559.

23 W. T. Wu, H. Jiang, Y. T. Qi, W. T. Fan, J. Yan, Y. L. Liu and W. H. Huang, *Angew. Chem., Int. Ed.*, 2021, **60**, 19337–19343.

24 X. L. He and A. G. Ewing, *J. Am. Chem. Soc.*, 2020, **142**, 12591–12595.

25 H. Y. Wang, Y. F. Ruan, L. B. Zhu, X. M. Shi, W. W. Zhao, H. Y. Chen and J. J. Xu, *Angew. Chem., Int. Ed.*, 2021, **60**, 13244–13250.

26 A. M. Vargason, A. C. Anselmo and S. Mitragotri, *Nat. Biomed. Eng.*, 2021, **5**, 951–967.

27 W. Zhao and J. J. Xu, *Chin. J. Chem.*, 2022, **40**, 1975–1986.

28 Y. L. Wang, R. Jin, N. Sojic, D. Jiang and H. Y. Chen, *Angew. Chem., Int. Ed.*, 2020, **59**, 10416–10420.

29 H. Y. Wang, Y. T. Xu, B. Wang, S. Y. Yu, X. M. Shi, W. W. Zhao, D. Jiang, H. Y. Chen and J. J. Xu, *Angew. Chem., Int. Ed.*, 2022, **61**, e202212752.

30 Y. T. Xu, Y. F. Ruan, H. Y. Wang, S. Y. Yu, X. D. Yu, W. W. Zhao, H. Y. Chen and J. J. Xu, *Small*, 2021, **17**, 2100503.

31 T. Y. Zhang, S. Y. Yu, B. Wang, Y. Xu, X. Shi, W. Zhao, D. Jiang, H. Chen and J. Xu, *Research*, 2022, **2022**, 9859101.

32 X. M. Shi, Y. T. Xu, B. Y. Zhou, B. Wang, S. Y. Yu, W. W. Zhao, D. Jiang, H. Y. Chen and J. J. Xu, *Angew. Chem., Int. Ed.*, 2023, **62**, e202215801.

33 A. J. Bard and L. R. Faulkner, Electrochemical Methods: Fundamentals and Applications, 1980.

34 B. Xiong, R. Zhou, J. Hao, Y. Jia, Y. He and E. S. Yeung, *Nat. Commun.*, 2013, **4**, 1708.

35 K. H. Xu, D. R. Luan, X. T. Wang, B. Hu, X. Liu, F. Kong and B. Tang, *Angew. Chem., Int. Ed.*, 2016, **55**, 12751–12754.

36 O. Kabil and R. Banerjee, *Antioxid. Redox Signaling*, 2013, **20**, 770–782.

37 V. S. Lin, W. Chen, M. Xian and C. J. Chang, *Chem. Soc. Rev.*, 2015, **44**, 4596–4618.

38 R. E. Ozel, G. Bulbul, J. Perez and N. Pourmand, *ACS Sens.*, 2018, **3**, 1316–1321.

39 S. H. Park, N. Kwon, J. H. Lee, J. Yoon and I. Shin, *Chem. Soc. Rev.*, 2020, **49**, 143–179.

40 Y. Sun, S. Chen, X. Y. Chen, Y. L. Xu, S. Y. Zhang, Q. Ouyang, G. Yang and H. Li, *Nat. Commun.*, 2019, **10**, 1323.

41 E. Pozo Guisado, A. Alvarez Barrientos, S. Mulero Navarro, B. Santiago Josefat and P. M. Fernandez Salguero, *Biochem. Pharmacol.*, 2002, **64**, 1375–1386.

42 A. D. Michel, M. Xing and P. P. A. Humphrey, *Br. J. Pharmacol.*, 2001, **132**, 1501–1508.